Published in "Physical Review A 74: 032509, 2006"
which should be cited to refer to this work.

Rb^*He_n exciplexes in solid ^4He

A. Hofer,* P. Moroshkin, D. Nettels, S. Ulzega, and A. Weis
Département de Physique, Université de Fribourg, Chemin du Musée 3, 1700 Fribourg, Switzerland

We report the observation of emission spectra from Rb^*He_n exciplexes in solid ^4He. Two different excitation channels were experimentally identified, viz., exciplex formation via laser excitation to the atomic $5P_{3/2}$ and to the $5P_{1/2}$ levels. While the former channel was observed before in liquid helium, on helium nanodroplets, and in helium gas by different groups, the latter creation mechanism occurs only in solid helium or in gaseous helium above 10 K. The experimental results are compared to theoretical predictions based on the extension of a model, used earlier by us for the description of Cs^*He_n exciplexes. We also report the observation of fluorescence from atomic rubidium in solid helium, and discuss striking differences between the spectroscopic features of Rb-He and Cs-He systems.

I. INTRODUCTION

The formation process of alkali-metal–He_n exciplexes, i.e., of bound states of an excited alkali-metal atom with one or more ground-state helium atoms, was studied in recent years in superfluid [1,2] and in solid [3] helium. These studies have given support to earlier proposals [4,5], which tentatively explained the quenching of atomic fluorescence from light alkali-metal atoms (Li, Na, K) in condensed helium by the formation of alkali-metal–helium exciplexes, whose emission spectra are strongly redshifted with respect to the atomic resonance lines. Exciplex formation was also studied on the surface of helium nanodroplets [6–10] and in cold helium gas [1,2,11]. Recently we have performed an experimental and theoretical study of the Cs^*He_n exciplex formation process in the hcp and bcc phases of solid ^4He [12]. A comparison with the results of [1,2] has revealed that the exciplex formation mechanism in solid helium differs from the one in superfluid helium and in cold helium gas. We concluded that exciplexes in solid helium result from the collective motion of several nearby helium atoms which approach the Cs atom simultaneously, while in liquid and gaseous helium the binding of the helium atoms proceeds in a time-sequential way.

The motivation for the present study of the Rb-He system arose from the question whether the collective mechanism is specific for Cs in solid helium, or whether it also holds for other alkali-metal atoms. While the light alkali-metal atoms (Li, Na, K) do not emit resonance fluorescence when excited in condensed helium, atomic cesium fluoresces both in superfluid and in solid helium, when excited on the D_1 transition. Rubidium represents an intermediate case, as it was reported [13] to fluoresce in liquid helium when excited on the D_1 transition with a yield which is strongly quenched with increasing He pressure. No fluorescence from Rb in solid helium was observed in the past, although it was shown that optically detected magnetic resonance can be used to detect light absorption on its D_1 transition [14].

A major difference between cesium and rubidium exciplexes Rb (Cs) $(A\,^2\Pi_{1/2})He_n$ becomes apparent from Fig. 1 which shows the calculated binding energies ϵ_b(Rb) [ϵ_b(Cs)] of the exciplexes as a function of the number n of bound helium atoms for Rb (Cs). For Cs only exciplexes with five, six, and seven helium atoms have their energy below the dissociation limit and are therefore stable, while for Rb all exciplexes with $n=1,\ldots,8$ are stable.

For cesium the binding energy has a local minimum for $n=2$ (quasibound complex) and there is a potential barrier that hinders the formation of exciplexes with more than two helium atoms in a sequential manner. As evidenced by the measurements of [1] the $Cs^*He_{n=2}$ exciplex is therefore the largest complex that can be formed by a sequential attachment of He atoms. Larger complexes can only be formed in a collective way, which becomes possible in pressurized solid helium [3]. The largest stable complex will be the one

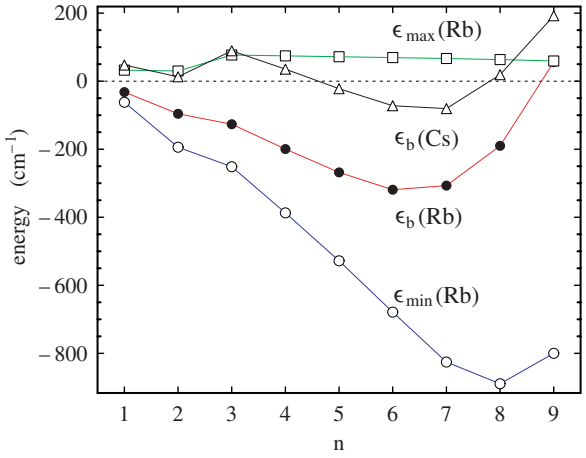

FIG. 1. (Color online) Calculated energies of Rb$(A\,^2\Pi_{1/2})He_n$ exciplexes as a function of the number n of attached helium atoms. All energies [defined in Fig. 2(b)] are given with respect to the dissociation limit, i.e., the energy of the $5P_{1/2}$ state of free Rb. Shown here are the depths of the potential wells ϵ_{min}(Rb) (open circles), the barrier heights ϵ_{max}(Rb) (open squares), and the binding energies ϵ_b(Rb) (solid dots). The binding energies ϵ_b(Cs) (open triangles) of Cs exciplexes from [12] are shown for comparison.

*Electronic address: adrian.hofer@unifr.ch
†URL: www.unifr.ch/physics/frap/

with the lowest binding energy. For Rb all the exciplexes with $n=1,\ldots,8$ are stable, so once the $Rb^*He_{n=1}$ exciplex is created all larger complexes can be formed with high probability by the sequential filling of the helium ring until the state with the lowest binding energy is reached. In helium environments with lower densities than pressurized solid helium the time interval between successive attachments is long enough to permit the exciplex to fluoresce, so that fluorescence from all intermediate exciplexes $Rb^*He_{n=1,\ldots,6}$ can be observed in gaseous helium [2]. The results presented below indicate that in solid He the $Rb(A\,^2\Pi_{1/2})He_n$ formation process is so rapid that any intermediate configurations have no time to emit fluorescence. For Rb in solid helium one therefore expects that only the most strongly bound Rb^*He_6 exciplex is formed.

In Sec. II we review the theoretical model for the description of exciplex spectra developed in [12] and extend it to the Rb-He system. In Sec. III we introduce the experimental setup and present experimental emission and excitation spectra of rubidium-helium exciplexes. In Sec. IV we compare the experimental results with the theoretical model calculations as well as other experiments and discuss the different decay channels of excited Rb in solid helium.

II. THEORY

We briefly describe the theoretical approach of our calculation of the Rb^*He_n exciplex emission spectra for $n=1-9$. The model used is an extension of the calculations performed earlier for cesium-helium exciplexes [3,12] and we shall review only the basic principles and assumptions. We consider only the interaction of the excited Rb atom with the n helium atoms that form the exciplex and neglect the influence of the helium bulk. The largest perturbation comes from the close helium atoms that form the exciplex and it is therefore a good approximation to neglect the helium bulk. The interaction between the Rb atom and one ground state helium atom is described as a sum over semiempirical pair potentials [15]

$$V_n^{\text{Rb-He}}(r)=\sum_{i=1}^{n} V^{5P}(\mathbf{r}_i), \qquad (1)$$

where $\mathbf{r}_i$ is the position of the ith helium atom with respect to the position of the Rb atom. After including the spin-orbit interaction of the Rb valence electron and the helium-helium interaction $V_n^{\text{He-He}}(r)$ modeled as the sum over interaction potentials [16] between neighboring helium atoms, the total interaction Hamiltonian is given by

$$V_{\text{Rb}^*\text{He}_n}(r)=V_n^{\text{Rb-He}}(r)+V_n^{\text{He-He}}(r)+(2/3)\Delta\mathbf{L}\cdot\mathbf{S}, \qquad (2)$$

where $\Delta=237.6\ \text{cm}^{-1}$ is the fine-structure splitting of the rubidium $5P$ state in the free atom. $\mathbf{L}$ is the orbital angular momentum operator and $\mathbf{S}$ the electronic spin operator. Next, the total interaction operator $V_{\text{Rb}^*\text{He}_n}(r)$ is represented in the basis $|n,L,S\rangle$ and diagonalized algebraically. Exciplexes of two different structures are formed as in the case of cesium-helium exciplexes. When one or two helium atoms are bound the electronic wave function has an apple shape with the helium atoms attached in its dimples, whereas for $n>2$ the electronic wave function has a dumbbell shape, with the bound helium atoms distributed along a ring around the dumbbell's waist. The potential curves leading to the formation of these two classes of structures are represented in Fig. 2 using the examples of Rb^*He_2 and Rb^*He_6. The potential curves shown represent the r-dependent eigenvalues of the operator $V_{\text{Rb}^*\text{He}_n}(r)$ of Eq. (2). In the same figures we also show the ground-state potentials $nV_\sigma^{5S}(r)+V_n^{\text{He-He}}(r)$. We will

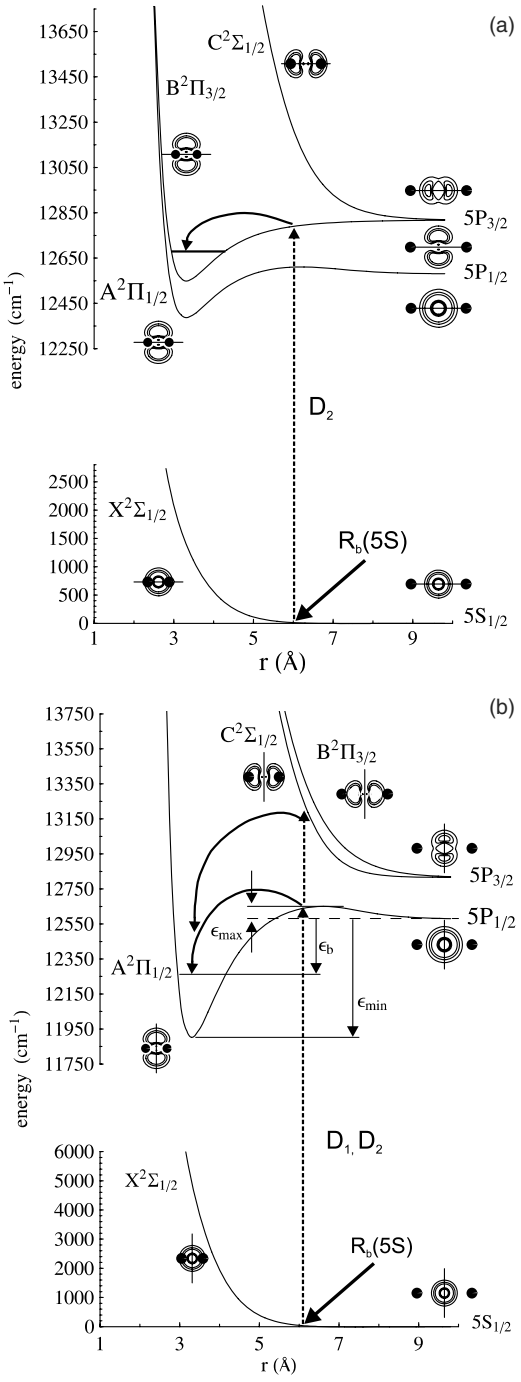

FIG. 2. Adiabatic potentials of the Rb^*He_n system: (a) Rb^*He_2, (b) Rb^*He_6. The equilibrium bubble radius of the ground-state Rb atom is indicated with $R_b(5S)$. The energies shown in Fig. 1 as a function of the number of bound helium atoms are visualized in (b).

use the standard spectroscopic notation ($X\,^2\Sigma_{1/2}$, $A\,^2\Pi_{1/2}$, $B\,^2\Pi_{3/2}$, and $C\,^2\Sigma_{1/2}$) also for complexes with $n>2$ for simplicity and to be consistent with our previous publications [3,12] although this notation is, strictly speaking, valid only for linear molecules.

As can be seen from Fig. 2(a) the energetically most favorable formation channel for Rb^*He_2 proceeds via D_2 excitation; when two helium atoms approach along the nodal line of the apple-shaped electron distribution of the $B\,^2\Pi_{3/2}$ state, they are attracted into the potential minimum. When the system is excited on the D_1 transition the approaching helium atoms experience a repulsive spherical electronic distribution of the Rb atom at large distances with a potential barrier of 29 cm^{-1}. We recall that the corresponding barrier height in cesium is 79 cm^{-1} [12] due to the larger spin-orbit interaction energy in that atom [4]. The approaching helium atoms deform the electronic configuration of the $5P$ state from spherical to apple shaped.

The exciplexes with $n>2$ [Fig. 2(b)] have no potential well in the $B\,^2\Pi_{3/2}$ state, which is purely repulsive and which correlates with the $5P_{3/2}$ atomic state. However, the $A\,^2\Pi_{1/2}$ state possesses a potential well and a potential barrier. The barrier is associated with the transformation of the electronic wave function from spherical to dumbbell shaped when several helium atoms approach the Rb atom. Exciplexes with $n>2$ can only be formed in the $A\,^2\Pi_{1/2}$ state.

The electronic distributions of the rubidium-helium system for the different states at various interatomic separations are illustrated by pictographs in Fig. 2. The solid lines represent the quantization axis, which is the internuclear axis for $Rb^*He_{n\leq 2}$ and the symmetry axis of the helium ring for the $Rb^*He_{n>2}$ complexes, while helium atoms are drawn as filled disks with a radius of 3.5 Å.

In a next step we have calculated the vibrational zero-point energies for all Rb^*He_n for $n=1,\ldots,9$. Details of this calculation were discussed in [12] for the case of cesium. Only the lowest vibrational state is considered as higher vibrational states are not populated at the temperature ($T=1.5$ K) of the experiment. A more detailed discussion about this statement will be given in Sec. IV B. The binding energies ϵ_b(Rb), ϵ_b(Cs), the well depths ϵ_{min}(Rb), and the barrier heights ϵ_{max}(Rb) are shown in Fig. 1 for $Rb(A\,^2\Pi_{1/2})He_{n=1,\ldots,9}$.

As a last step we calculate the emission spectra $I(\nu)$ of all $Rb^*He_{n=1,\ldots,9}$ exciplexes under the Franck-Condon approximation as discussed in [12]. The theoretical emission spectra for $Rb(B\,^2\Pi_{3/2})He_{n=1,2}$ and for $Rb(A\,^2\Pi_{1/2})He_{n=6,7}$ are shown in Fig. 3.

III. EXPERIMENTAL RESULTS

A. Experimental setup

The experimental setup is similar to the one described in our previous publication [3]. A helium crystal is grown at pressures around 30 bar in a pressure cell immersed in superfluid helium at 1.5 K. The matrix is doped with rubidium atoms by laser ablation using a frequency-doubled neodymium-doped yttrium aluminum garnet (Nd:YAG) laser. The cell has five windows for admitting the ablation beam and the beam of the spectroscopy laser (a tunable cw $Ti:Al_2O_3$ laser) and for collecting fluorescence from the sample volume. The fluorescence is dispersed by a grating spectrometer and recorded, depending on the spectral range under investigation, either by a charge-coupled device (CCD) camera (9500–13 500 cm^{-1}) or by an $In_xGa_{1-x}As$ photodiode (5500–9500 cm^{-1}). We shall refer to these as the CCD spectrometer and $In_xGa_{1-x}As$ spectrometer, respectively. With the $In_xGa_{1-x}As$ spectrometer spectra were recorded by a stepwise tuning of the grating, while integral spectra could be recorded with the CCD spectrometer.

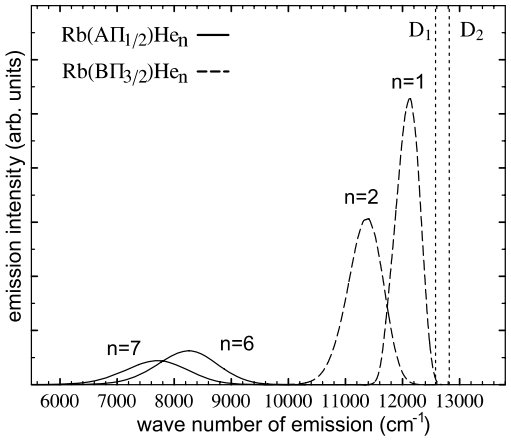

FIG. 3. Calculated emission spectra of $Rb(B\,^2\Pi_{3/2})He_{n=1,2}$ (dashed lines) and $Rb(A\,^2\Pi_{1/2})He_{n=6,7}$ (solid lines). The dotted lines indicate the positions of the resonance lines of the free Rb atom.

B. Atomic bubbles

Defect atoms in solid helium reside in atomic bubbles, whose size and structure can be described by the equilibrium between a repulsive alkali-metal–helium interaction due to the Pauli principle on one hand and surface tension and pressure volume work on the other hand [5,17,18]. The interaction with the helium bulk shifts the $5S_{1/2}\rightarrow 5P_{1/2}$ (D_1) and $5S_{1/2}\rightarrow 5P_{3/2}$ (D_2) transitions of Rb by approximately 35 nm to the blue with respect to their values (794 and 780 nm, respectively) in the free atom. This shift of the excitation lines as well as a smaller blueshift of the corresponding emission lines is well described by the bubble model [5,19]. We have calculated the equilibrium radius of the atomic bubble formed by the $5S_{1/2}$ ground state of the Rb atom to be $R_b=6$ Å (Fig. 2) following the model described in [17,18]. For the interaction potential between ground-state Rb and He atoms we have used the same semiempirical potentials [15] as for the exciplex model.

It is the close vicinity of the helium atoms in the first solvation shell, together with their large zero-point oscillation amplitudes, that form the basis of the efficient exciplex formation in solid helium.

C. Emission spectra following D_1 excitation

Figure 4 shows the emission spectrum recorded with the CCD spectrometer following excitation at the D_1 wavelength

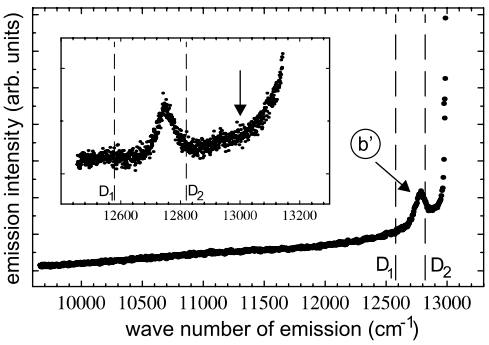

FIG. 4. Measured emission spectrum (dots) recorded with the CCD spectrometer following D_1 excitation. The dashed vertical lines indicate the D_1 and D_2 lines of the free Rb atom. The peak b' is the fluorescence from the D_1 transition. The inset shows the spectral range around the D lines recorded with a higher-resolution grating and an excitation frequency slightly (65 cm^{-1}) shifted to the blue. The rise on the right side is from scattered laser light. The arrow gives the position at which D_2 emission is detected after D_2 excitation (peak a in Fig. 6 below).

13 140 cm^{-1} (758 nm). The peak b' at 12 780 cm^{-1} represents fluorescence from the atomic $5P_{1/2}$ state. While D_1 atomic fluorescence from Cs in solid helium has been studied and used extensively in the past it was believed that rubidium would not fluoresce on the D_1 transition when embedded in solid helium. This belief was based on the reported quenching of the atomic fluorescence at high pressures in superfluid helium [13]. It should be noted that the Rb D_1 fluorescence reported here is orders of magnitude weaker than the corresponding line in Cs and could only be detected with long integration times (4 s) of the CCD camera, which probably explains why this spectrum was not observed in previous experiments [14].

The apple-shaped exciplexes with one or two bound helium atoms are expected to fluoresce within the spectral range of Fig. 4 and the absence of any prominent spectral feature indicates that these complexes are not formed upon D_1 excitation. The sloped background visible in Figs. 4 and 6 is a strong wing of scattered laser light ($\lambda = 13\,160$ cm^{-1}). The inset in Fig. 4 shows a spectrum that was recorded using a grating with a higher resolution. The excitation laser was shifted by 65 cm^{-1} [still in the D_1 absorption band (Fig. 7 below)] to the blue with respect to the spectrum of Fig. 4 to make clear that no D_2 emission can be observed after D_1 excitation. The arrow in the inset indicates the position of the D_2 emission measured after D_2 excitation (peak a in Fig. 6).

When exploring the longer-wavelength range with the $In_xGa_{1-x}As$ spectrometer we found a very strong fluorescence band (Fig. 5) centered at 7420 cm^{-1}, which we assign to $Rb^*He_{n>2}$ exciplexes in the $A\,^2\Pi_{1/2}$ state. This is proof that the quenching of atomic D_1 fluorescence in rubidium [13] is due to exciplex formation. A similar emission following D_1 excitation has been observed in gaseous He above 10 K [2]. Measurements at lower He gas temperatures and measurements in liquid He at 1.8 K have shown no exciplex formation after D_1 excitation [2]. The question of why exciplex formation becomes possible again in solid He will be addressed in Sec. IV E. The dashed and the solid lines in Fig.

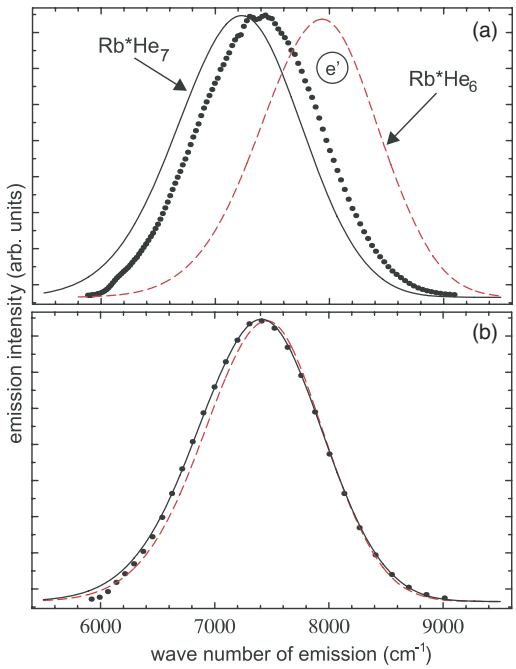

FIG. 5. (Color online) Fluorescence spectrum (dots) following D_1 excitation measured with the $In_xGa_{1-x}As$ spectrometer. The emission band stems from a $Rb^*He_{n>2}$ exciplex (e'). An identical emission spectrum was observed after D_2 excitation. (a) The dashed line is a calculated emission spectrum from Rb^*He_6 and the solid line from Rb^*He_7. (b) The two theoretical spectra are shifted in order to match the experimental curve.

5 are theoretical emission spectra from Rb^*He_6 and Rb^*He_7, respectively. Figure 5(b) shows the theoretical curves, shifted such as to make their blue wings coincide with the experimental points. The line shape of the experimental curve is well reproduced by the two theoretical curves. The theoretical curve of Rb^*He_7 fits the experimental points better on the low-energy side, while on the high-energy side both curves are in very good agreement with the experimental spectrum. A small discrepancy is visible on the low-energy wing, which can be due to imprecisions of the strongly sloped ground-state potential (Fig. 2) or to changes of the latter due to the helium bulk. It is a remarkable fact that the fluorescence yield of this exciplex after D_1 excitation in solid helium is larger than after D_2 excitation, while it was not observed at all in superfluid helium. We will come back to this point in Sec. III.

A similar emission at around 7200 cm^{-1} has been seen in liquid helium by Hirano *et al.* [2] after D_2 excitation and was assigned to the emission by the Rb^*He_6 exciplex.

D. Emission spectra following D_2 excitation

Figure 6 shows the emission spectrum, measured with the CCD spectrometer, when the laser is tuned to the atomic D_2 transition at 13 420 cm^{-1} (745 nm).

Four prominent spectral features can be seen in the emission spectrum. The two rightmost peaks (labeled a and b) represent atomic D_2 and D_1 fluorescence, respectively. Together with the peak of Fig. 4 they constitute the observation

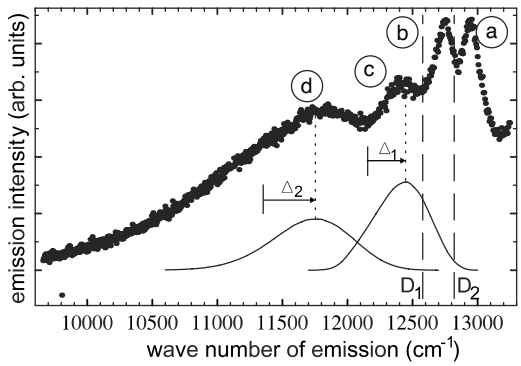

FIG. 6. Fluorescence spectrum (dots) recorded with the CCD spectrometer following D_2 excitation. The dashed vertical lines indicate the positions of the D_1 and D_2 lines of the free Rb atom. The following assignments are made to the emission peaks: atomic D_2 fluorescence (a), atomic D_1 fluorescence (b), emission from Rb($B\,^2\Pi_{3/2}$)He$_1$ exciplexes (c), and emission from Rb($B\,^2\Pi_{3/2}$)He$_2$ exciplexes (d). The solid lines are calculated emission spectra from Rb($A\,^2\Pi_{3/2}$)He$_1$ and Rb($A\,^2\Pi_{3/2}$)He$_2$ exciplexes. The lines are shifted in order to match the peaks of the experimental curves. Δ_1=350 cm^{-1} and Δ_2=440 cm^{-1} are the shifts with respect to the calculated positions shown in Fig. 3.

of atomic fluorescence from rubidium in solid helium. The presence of D_1 emission after D_2 excitation is evidence for the existence of a fine-structure relaxation channel. We assign the two broader features c and d peaked at 12 400 and 11 800 cm^{-1}, respectively, to the emission from Rb($B\,^2\Pi_{3/2}$)He$_1$ and Rb($B\,^2\Pi_{3/2}$)He$_2$ exciplexes. The solid lines in Fig. 6 are the calculated n=1 and 2 emission spectra of Fig. 3 shifted to the blue by Δ_1 and Δ_2, respectively, so that their line centers coincide with the positions of the measured curves. The shifts are probably due to the interaction with the surrounding helium bubble. Note that the two theoretical curves have to be shifted by different amounts in order to match the experimental lines. We have found previously in the Cs-He system [12] that the rate and sign of the pressure shift of exciplex emission lines depend on the number of bound helium atoms.

As with the spectra of Sec. III C we have recorded the emission in the region of longer wavelengths with the In$_x$Ga$_{1-x}$As spectrometer. As a result we find a spectrum that is identical (same central wavelength and same width) with the one observed with D_1 excitation (Fig. 5). This suggests that the emission stems from the same state ($A\,^2\Pi_{1/2}$) as the emission after D_1 excitation. The population of that state following D_2 excitation is another proof of the existence of a fine-structure relaxation mechanism. No other exciplex emission was observed in the spectral range between the Rb*He$_{n>2}$ and the Rb*He$_2$ exciplex emissions [peak e' in Fig. 5(a) and peak d in Fig. 6, respectively].

E. Atomic and exciplex excitation spectra

The experimental emission spectra presented above were recorded with two fixed excitation wavelengths, chosen such as to maximize the signals of interest. It is of course interesting to investigate how the different spectral features de-

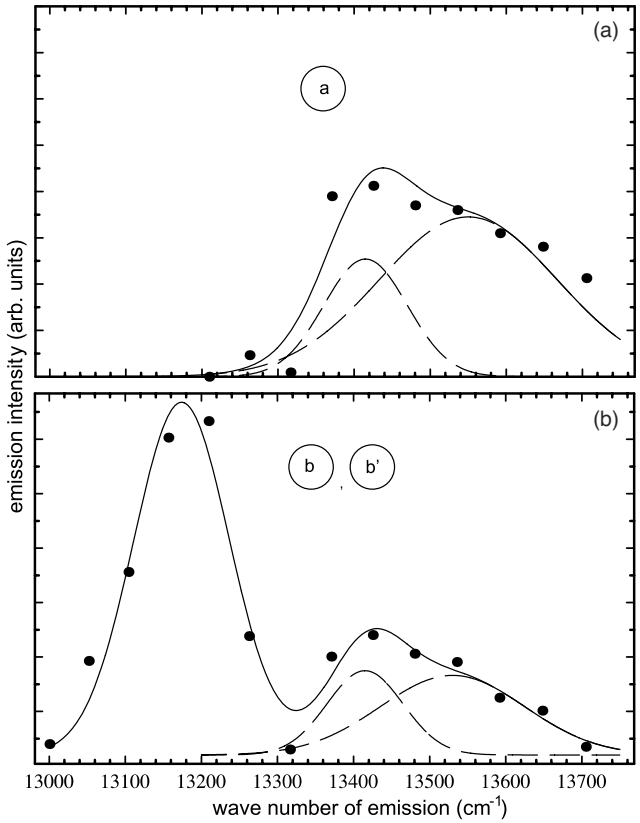

FIG. 7. Excitation spectra of the fluorescence from atomic rubidium. Top: fluorescence analyzing spectrometer set to the D_2 emission line (peak a of Fig. 6). Bottom: spectrometer set to the D_1 emission line (peaks b' and b of Figs. 4 and 6). The dashed lines are Gaussians whose sum (solid line) was fitted to the data.

pend on the excitation wavelength. For this we have varied the wavelength of the Ti:Al$_2$O$_3$ laser in discrete steps over the spectral range of 13 000–13 700 cm^{-1} (~770–730 nm). For every excitation wavelength we have measured the amplitudes of the emission peaks of Figs. 4–6.

The top part of Fig. 7 shows the excitation spectrum of D_2 fluorescence, which is centered at 13 460 cm^{-1} (743 nm). One sees clearly that this fluorescence can only be produced by D_2 excitation. The lower part of Fig. 7 shows the excitation spectrum of D_1 fluorescence. It consists of two absorption bands centered at 13 180 and 13 460 cm^{-1}, respectively, which correspond to excited states correlating with the atomic $5P_{1/2}$ and $5P_{3/2}$ levels, respectively. D_1 fluorescence can thus be produced directly via D_1 excitation or via D_2 excitation combined with a J-mixing interaction due to the alkali-metal–helium interaction.

The D_1 absorption band is slightly asymmetric with a longer wing on the low-energy side. This feature has been observed before in Cs [5]. The D_2 absorption band measured for both D_1 and D_2 fluorescence has a double-peaked structure. The scarce number of data points is well fitted by a superposition of two Gaussians separated by about 125 cm^{-1}. This splitting of the D_2 excitation lines of cesium and rubidium in superfluid helium has been explained before in terms of a dynamic Jahn-Teller effect due to quadrupolar bubble-shape oscillations which lift the degeneracy of the $P_{3/2}$ state [20].

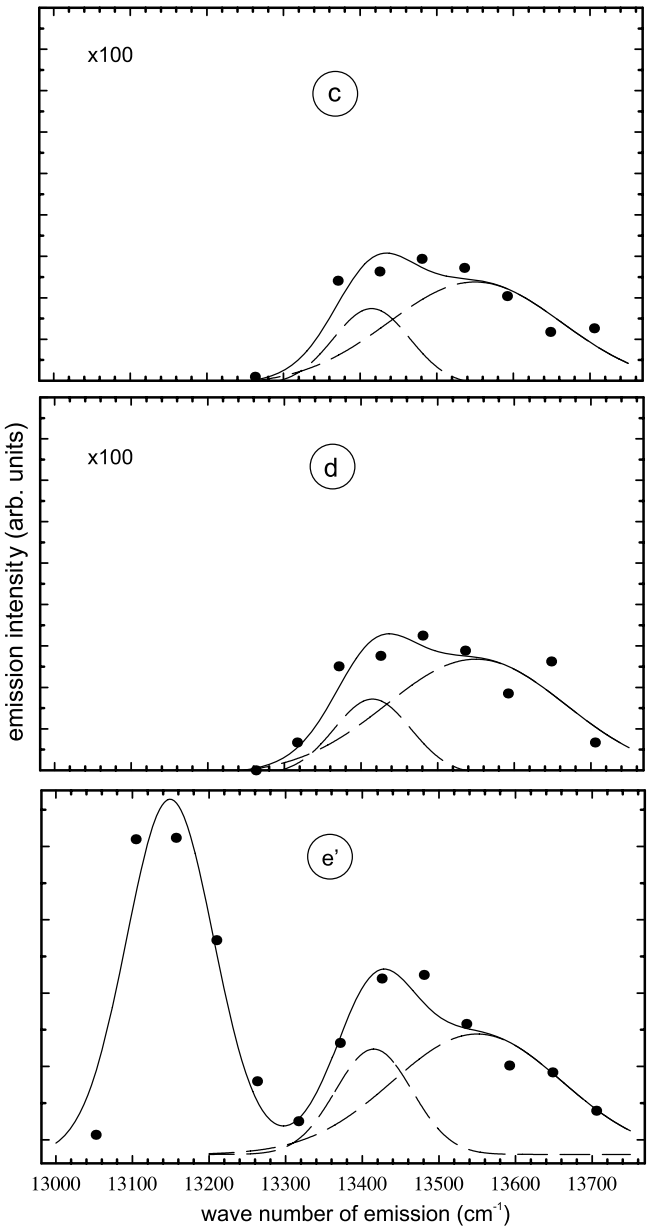

FIG. 8. Excitation spectra of the fluorescence from Rb^*He_n exciplexes (dots) with the fluorescence spectrometer tuned to emission from Rb^*He_1 *c*, Rb^*He_2 *d*, and $Rb^*He_{n_{max}}$ e'. The solid lines are Gaussian fits. The signal in the spectrum e' is approximately two orders of magnitude larger than the ones of *c* and *d* and than the atomic signals from Fig. 7.

Figure 8 shows the excitation spectra of the exciplex lines *c*, *d*, and e' of Figs. 5 and 6. As the $Rb^*He_{1,2}$ exciplexes can only be observed after D_2 excitation (Fig. 8 curves *c* and *d*) we conclude that these apple-shaped complexes are formed in the $B\ ^2\Pi_{3/2}$ state. The D_1, D_2, and $Rb(B\ ^2\Pi_{3/2})He_{1,2}$ emission lines are very weak and of similar amplitude. The bottom spectrum (e') represents by far the strongest signal that comes from the $Rb(A\ ^2\Pi_{1/2})He_{n>2}$exciplex which can be excited by either D_1 or D_2 radiation. Its emission line is about 100 times stronger than the other lines. This result is in strong contrast with the emission of the corresponding cesium exciplex $Cs(A\ ^2\Pi_{1/2})He_{n>2}$ in solid helium, for which the emission after D_1 excitation is very weak [12]. The double-peaked structure of the D_2 excitation spectrum is not well resolved for the $Rb^*He_{1,2}$ exciplexes. It was observed before for Cs^*He and Rb^*He exciplexes on superfluid helium nanodroplets [6,8].

IV. DISCUSSION

A. Atomic lines

The assignment of the atomic D_1 and D_2 excitation and emission lines is unambiguous. The excitation lines are blueshifted by approximately 600 cm^{-1}, while the emission lines are shifted by only 65 cm^{-1} with respect to the free-atomic transitions. These shifts (except that of the D_2 emission) have been studied in superfluid helium [18] and are well described by the bubble model. The blueshift results from the interaction with the bulk helium, which is less pronounced in the emission process as the latter occurs in a bubble of larger size [5].

As already mentioned, excitation at the D_1 transition leads to emission on the D_1 line only, while excitation at the D_2 line leads to emission on both the D_1 and the D_2 lines. It should be noted here that in liquid He [18] even under D_2 excitation one can only observe D_1 emission. We also recall that in Cs-doped condensed He D_2 emission is absent in both the liquid [18] and solid [12] phases. The absence of the D_2 emission from heavy alkali-metal atoms in condensed He is explained [1,2,12] by the very efficient formation of alkali-metal–helium exciplexes—a general phenomenon observed in the present study as well. We will return to this point in Sec. IV C.

B. Apple-shaped $Rb(B\ ^2\Pi_{3/2})He_{1,2}$ exciplexes

As one can see in Fig. 2(a), one or two helium atoms approaching the apple-shaped atomic $5P_{3/2}$, $m_J=\pm 3/2$ state do not experience a potential barrier on their way to the potential well of the $B\ ^2\Pi_{3/2}$ state. The formation process of Rb^*He_1 and Rb^*He_2 exciplexes is therefore straightforward after D_2 excitation. Note that the potential diagram for Rb^*He_1 is similar to the one for Rb^*He_2, shown in Fig. 2, with the difference that it has a reduced potential well depth. The $Rb^*He_{1,2}$ exciplex emission line following D_1 excitation is not observed because only the largest exciplex is formed as discussed in Sec. IV E.

Emission spectra very similar to the one in Fig. 6 have been previously observed in gaseous He below 2.1 K [2] and in Rb-doped He droplets [8]. The authors of [2] and [8] assigned their observations to the emission of several vibrational states of the $Rb(B\ ^2\Pi_{3/2})He_1$ and $Rb(A\ ^2\Pi_{1/2})He_1$ exciplexes. Their calculations of emission spectra support this assignment. However, we believe that in solid He at 1.5 K only the lowest vibrational state is populated and that we observe indeed the emission from two different exciplexes. The reasons are the following. The authors of [1,2] have shown that the higher vibrational states of the Rb^*He_1 and Cs^*He_1 exciplexes are only populated at low He gas densities. For higher densities, especially in liquid He, the collision-induced relaxation rate increases and only the low-

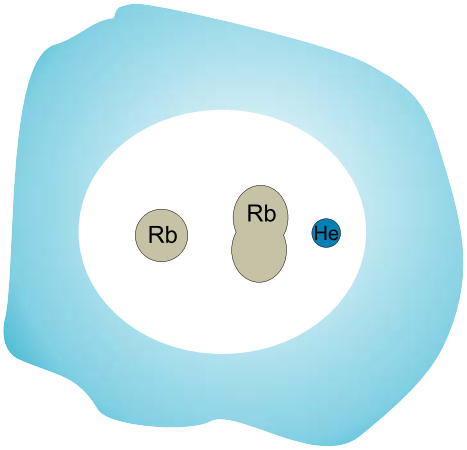

FIG. 9. (Color online) Sketch of a diatomic bubble after photodissociation of a Rb_2 dimer. A spherical ground-state Rb atom and an apple-shaped excited Rb atom share one bubble. Helium atoms can approach only from one side; thus formation of the Rb^*He_1 exciplex and its fluorescence becomes possible.

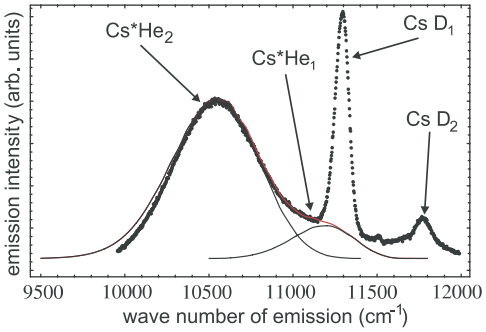

FIG. 10. (Color online) Spectrum (dots) observed upon photodissociation of the Cs_2 dimer. One can clearly identify the Cs D_1, D_2, and Cs^*He_2 emission lines. The Cs^*He_1 emission is very weak and results in a broadening of the Cs^*He_2 emission line. The black solid lines are calculated emission lines for the two smallest Cs exciplexes. They are shifted in order to fit the data points. The red (gray) line is a superposition of the two calculated lines.

est vibrational state is populated. The same mechanism should be even more efficient in solid He.

Our assignment of the peak c at 12 400 cm^{-1} in Fig. 6 to the emission from the lowest vibrational state of $Rb(B\,^2\Pi_{3/2})He_1$ agrees well with the experimental and theoretical results of [2,8], which place it at 12 000 cm^{-1}. Our measurements of the $Cs(B\,^2\Pi_{3/2})He_2$ exciplex [12] demonstrated a pressure-dependent blueshift with a rate of 10 cm^{-1}/bar and a sudden jump of 100 cm^{-1} at the bcc-hcp phase transition. Assuming similar shifts for the Rb^*He_1 exciplex, we can estimate the difference between the spectral position in liquid He at saturated vapor pressure and in our experiment at 30 bar to be on the order of 400 cm^{-1}.

The position of the peak d at 11 800 cm^{-1} is in good agreement with the position of the lowest vibrational state of $Rb(A\,^2\Pi_{1/2})He_1$ observed (and predicted) in [2,8] at 11 800–11 900 cm^{-1}. However, as we discuss in Sec. IV E, only the $Rb(A\,^2\Pi_{1/2})He_n$ exciplex with $n=n_{max}$ emits fluorescence in solid He and we expect the spectral position to be shifted with respect to the measurements in He gas. Therefore we assign this peak to the emission of $Rb(B\,^2\Pi_{3/2})He_2$, which according to our model is stable and should be present in the emission spectrum. Applying the same estimation of the pressure shift as described above one can expect that the emission of this complex in liquid He would be at 11 400 cm^{-1}, whereas the calculation of [2] places it at 10 900 cm^{-1}.At present we cannot explain this discrepancy.

Why the $Rb(B\,^2\Pi_{3/2})He_1$ exciplex is formed in solid He while the corresponding exciplex is not observed in Cs-doped solid He [12] is a more difficult question. We suggest a speculative interpretation in the following section.

C. Diatomic bubble

We next address the striking difference in the structure of the emission of Rb-doped solid He (present study) compared to Cs-doped condensed (liquid or solid) He [1,12,18]. More precisely, in the present study, under D_2 excitation we obtain D_1 and D_2 atomic Rb emission lines plus the emission of two apple-shaped exciplexes, whereas only D_1 atomic emission and one apple-shaped exciplex were observed in similar experiments with Cs.

In solid He the absorption and emission lines of atoms or molecules are shifted with respect to the value of the free species due to the interaction with the surrounding He bulk. The shift of the atomic lines is well understood in the framework of the bubble model. For Rb in solid He we have the particular situation that the atomic D_2 absorption line overlaps with a dissociative band $[(1)^3\Sigma_u \rightarrow (1)^3\Pi_g]$ of the Rb_2 dimer [21] also present in the same sample. We speculate that after dissociation two Rb atoms (one in the ground and one in the excited state) share one bubble as shown by the sketch in Fig. 9. The excited Rb atom has an apple-shaped orbital and can bind two He atoms but the ground-state atom inhibits one binding site. This situation leads to the formation of the $Rb(B\,^2\Pi_{3/2})He_1$ exciplex. At the same time the larger bubble perturbs the excited Rb atom less than the more compact single-atomic bubble, which reduces the quenching efficiency and thus results in measurable D_2 emission.

It is natural to expect Cs_2 dimers to be present in our experiments with Cs-doped solid He. In a separate study [22] we have confirmed this expectation; however, we have found that the photodissociation spectrum of Cs_2 has no overlap with the absorption lines of atomic Cs. The fluorescence spectrum recorded upon photodissociation of Cs_2 molecules at 670 nm (14 925 cm^{-1}) is presented in Fig. 10, where one can see both D_1 and D_2 atomic lines together with the $Cs(B\,^2\Pi_{3/2})He_2$ exciplex and the much weaker, but still distinguishable, $Cs(B\,^2\Pi_{3/2})He_1$ exciplex. The solid lines represent the exciplex emission spectra calculated using the same approach as described in [12] and in the present paper.

D. Dumbbell-shaped $Rb(A\,^2\Pi_{1/2})He_{n>2}$ exciplexes

The emission line shown in Fig. 5 has the longest wavelength of all observed spectral lines and originates thus from

the lowest-lying bound state, i.e., the $A\ ^2\Pi_{1/2}$ state of Fig. 2(b). Note that all $Rb^*He_{n>2}$ exciplexes have similar potential curves with potential wells increasing with n. All of these structures have the shape of dumbbells, with the helium atoms bound around their waists [12]. Figure 5 also shows the calculated line shapes of the emission from Rb^*He_6 and Rb^*He_7. Disregarding shifts of the line centers the theoretical line shapes match the experimental spectrum quite well. The good matching of the linewidth in particular indicates that this emission is from a single exciplex species with a specific number of bound helium atoms and that it does not come from a superposition of different exciplexes. The shift of the lines is most likely due to the interaction with the helium bulk, which was not taken into account in our calculation. It is difficult to estimate whether the bulk shifts the line to the blue or to the red. One can therefore not assign the observed emission band to Rb^*He_6 or Rb^*He_7 in an unambiguous way. The calculated binding energies ϵ_b(Rb) (Fig. 1) show that the complex with six helium atoms has the lowest binding energy and is therefore the most stable exciplex. Observations in liquid He [2] confirm this prediction. However, the exact calculation of the energy of the lowest-lying bound state involves a precise quantitative treatment of its oscillatory degrees of freedom. In [12] we have described in detail how we calculate these oscillation energies. There is an uncertainty in the calculated binding energies due to the simplified assumptions we made. An additional uncertainty comes from the semiempirical pair potentials [15]. For big exciplexes like the Rb^*He_6 every uncertainty in the potential will be amplified because of the additive contribution of the n helium atoms discussed in Sec. II. This can change the position and the depth of the well in the excited state. To all of this is added the effect of the helium bulk, which was not treated so far. The following arguments support that Rb^*He_6 is the structure observed. It has the minimal binding energy and the corresponding Cs exciplex line is shifted to lower wave numbers with increasing pressure [12]. Assuming the same tendency for the Rb exciplex brings the spectral position of Rb^*He_6 into better agreement with the experimental curve (Fig. 5). On the other hand, the line shape of the calculated Rb^*He_7 fits the data better. Therefore we cannot conclude which exciplex is the one observed in the experiment.

E. Formation of dumbbell-shaped $Rb(A\ ^2\Pi_{1/2})He_{n>2}$ exciplexes

The radius of the bubble formed by the rubidium ground state has an equilibrium radius R_b of 6 Å, which is smaller than the corresponding radius for cesium. The excitation process is a Franck-Condon transition to the $5P$ state during which the radius does not change.

The D_1 excitation starting at $R_b(5S)=6$ Å ends at the left of the potential barrier of the $A\ ^2\Pi_{1/2}$ state so that the exciplex is easily formed by helium atoms dropping into the well. Note that for cesium in solid helium the corresponding transition ends on the right side of the potential barrier in the excited state [12]. In that case the helium atoms have to tunnel through the potential barrier in order to form the exciplex. This explains why exciplex emission of Cs in solid helium after D_1 excitation is much weaker than after D_2 excitation, while for Rb the opposite holds. It also explains why no emission from Rb exciplexes after D_1 excitation could be observed in gaseous (below 10 K) and in liquid helium environments [2] in which the helium atoms are, on average, further away from the Rb atom and where the excitation thus ends at the right of the potential barrier. Under those conditions the exciplex formation is strongly suppressed as the helium atoms have to tunnel through the potential barrier to form the exciplex. This tunneling occurs at a rate that is smaller than the exciplex lifetime. The same is true for Rb on He droplets, where no exciplex was observed after D_1 excitation [10]. The authors of [10] estimated the tunneling time to be about 500 ns, much longer than the lifetime. Only for higher He gas temperatures (above 10 K) does the exciplex formation become possible again because the He atoms have enough kinetic energy to overcome the potential barrier.

When exciting the system at $R_b(5S)=6$ Å on the D_2 transition the corresponding fine-structure relaxation channel allows the system to form the terminal exciplex in the potential well of the $A\ ^2\Pi_{1/2}$ state.

In solid helium only the largest exciplex $Rb^*He_{n_{max}}$ is observed after D_1 excitation. This means that the potential well is filled up to the maximal value of helium atoms that it can hold on a time scale which is shorter than the radiative lifetimes of the intermediate products. It is therefore likely, as we have previously assumed for the formation of the corresponding cesium exciplexes, that the exciplex results from a collective motion of the helium atoms. The difference from the experiments in gaseous He is that in those experiments at any temperature not only the terminal exciplex but also transient products were observed [2].

F. Summary and conclusion

We have presented several additional spectral features observed in the laser-induced fluorescence from a helium crystal doped by laser ablation from a solid rubidium target. We detected weak but unambiguously identified D_1 and D_2 fluorescence lines from atomic rubidium, which were previously believed to be completely quenched in solid helium. We have shown that Rb^*He_n exciplex formation is possible after D_1 excitation, in contrast to cesium-doped solid He, in which exciplex formation proceeds mainly via absorption on the D_2 transition. We have explained this in terms of the smaller bubble diameter of rubidium, which allows the excitation to proceed directly to a binding state without tunneling processes as are needed with cesium. We have further reported the observation of $Rb^*He_{1,2}$ exciplex emission after D_2 excitation, a process that could not be observed in liquid helium. Our study has clearly confirmed that there are marked differences between the spectroscopy of Rb in gaseous He and in solid He. From the point of view of model calculations liquid and solid He should behave in a similar way. We have also observed a larger exciplex. The main decay channel of laser-excited Rb in solid helium is via the formation of this largest exciplex, assigned to be either Rb^*He_6 or Rb^*He_7, with subsequent emission of strongly redshifted fluorescence.

We proposed that the formation of a diatomic bubble could explain why we could observe the two exciplexes

Rb^*He_1 and Rb^*He_2, while in an equivalent experiment with cesium only the Cs^*He_2 complex was detected. This feature could be related to a recently discovered dissociation band of the Rb_2 dimer which overlaps with the D_2 atomic absorption line [21]. This interpretation in terms of the diatomic bubble may also explain the absence of the Rb^*He_1, Rb^*He_2, and D_2 emission in liquid He. Because of the preparation process in liquid He, the Rb_2 dimer density may be strongly reduced. On the other hand it could also be, that, due to the different pressure shifts, the dissociation band of Rb_2 and the atomic absorption lines no longer overlap in liquid He. More studies are needed to clarify this point. Besides purely spectroscopic studies, time-resolved femtosecond pump-probe experiments would be an additional helpful tool to elucidate this open question.

ACKNOWLEDGMENTS

We thank J. Pascale for sending us his numerical Rb-He pair potentials. This work was supported by the Grant No. 200020-103864 of the Schweizerischer Nationalfonds.

[1] K. Enomoto, K. Hirano, M. Kumakura, Y. Takahashi, and T. Yabuzaki, Phys. Rev. A **66**, 042505 (2002).
[2] K. Hirano, K. Enomoto, M. Kumakura, Y. Takahashi, and T. Yabuzaki, Phys. Rev. A **68**, 012722 (2003).
[3] D. Nettels, A. Hofer, P. Moroshkin, R. Müller-Siebert, S. Ulzega, and A. Weis, Phys. Rev. Lett. **94**, 063001 (2005).
[4] J. Dupont-Roc, Z. Phys. B: Condens. Matter **98**, 383 (1995).
[5] S. Kanorsky, A. Weis, M. Arndt, R. Dziewior, and T. Hänsch, Z. Phys. B: Condens. Matter **98**, 371 (1995).
[6] O. Bünermann, M. Mudrich, M. Weidemüller, and F. Stienkemeier, J. Chem. Phys. **121**, 8880 (2004).
[7] C. P. Schulz, P. Claas, and F. Stienkemeier, Phys. Rev. Lett. **87**, 153401 (2001).
[8] F. R. Brühl, R. A. Trasca, and W. E. Ernst, J. Chem. Phys. **115**, 10220 (2001).
[9] J. Reho, J. Higgins, C. Callegari, K. K. Lehmann, and G. Scoles, J. Chem. Phys. **113**, 9686 (2000).
[10] J. Reho, J. Higgins, K. K. Lehmann, and G. Scoles, J. Chem. Phys. **113**, 9694 (2000).
[11] K. Enomoto, K. Hirano, M. Kumakura, Y. Takahashi, and T. Yabuzaki, Phys. Rev. A **69**, 012501 (2004).
[12] P. Moroshkin, A. Hofer, D. Nettels, S. Ulzega, and A. Weis, J. Chem. Phys. **124**, 024511 (2006).
[13] T. Kinoshita, K. Fukuda, T. Matsuura, and T. Yabuzaki, Phys. Rev. A **53**, 4054 (1996).
[14] T. Eichler, R. Müller-Siebert, D. Nettels, S. Kanorsky, and A. Weis, Phys. Rev. Lett. **88**, 123002 (2002).
[15] J. Pascale, Phys. Rev. A **28**, 632 (1983).
[16] R. A. Aziz and A. R. Janzen, Phys. Rev. Lett. **74**, 1586 (1995).
[17] S. I. Kanorsky, M. Arndt, R. Dziewior, A. Weis, and T. W. Hänsch, Phys. Rev. B **50**, 6296 (1994).
[18] T. Kinoshita, K. Fukuda, Y. Takahashi, and T. Yabuzaki, Phys. Rev. A **52**, 2707 (1995).
[19] H. Bauer, M. Beau, B. Friedl, C. Marchand, K. Miltner, and H. J. Reyher, Phys. Lett. A **146**, 134 (1990).
[20] T. Kinoshita, K. Fukuda, and T. Yabuzaki, Phys. Rev. B **54**, 6600 (1996).
[21] P. Moroshkin, A. Hofer, S. Ulzega, and A. Weis, Phys. Rev. A **74**, 032504 (2006).
[22] P. Moroshkin, A. Hofer, S. Ulzega, and A. Weis, (unpublished).